

The influence of long-range transported pollution on the annual and diurnal cycles of carbon  
monoxide and ozone at Cheeka Peak Observatory

Peter Weiss-Penzias\* and Daniel A. Jaffe

Interdisciplinary Arts and Sciences, University of Washington, Bothell

Lyatt Jaeglé and Qing Liang

Department of Atmospheric Sciences, University of Washington, Seattle

Index Terms:0345, 0368, 0365

Submitted to Journal of Geophysical Research, Atmospheres, ITCT 2K2 Special Issue

\*Corresponding Author's telephone and email: (425) 352-3475, [pweiss@uwb.edu](mailto:pweiss@uwb.edu)

**Abstract.** We assess the importance of distant pollution sources on the marine background by combining measurements of carbon monoxide (CO) and ozone (O<sub>3</sub>) with model simulations from the GEOS-CHEM chemical transport model and two types of back trajectories. Measurements were made over a complete annual cycle from March 2001 to May 2002 at Cheeka Peak Observatory (CPO) in Washington State. Data from an earlier campaign (March-April 1997, 1998) were also incorporated. The seasonal cycles of CO and O<sub>3</sub> show a spring maximum and a summer minimum, consistent with other remote sites in the marine boundary layer (MBL). European and Asian pollution emission sources of CO, parameterized by GEOS-CHEM, were grouped into one category called “LRT” – representing “long-range transport”. LRT values produced good correlations with measured CO (monthly averaged  $r = 0.60$ , 6-hour averages) and were found to comprise between 15-60% of total CO, with higher values in winter/spring and lower in the summer/fall. CO and O<sub>3</sub> observations were classified based on these LRT values, creating two general categories – “more polluted” (LRT > 75<sup>th</sup> percentile from monthly distribution) and “less polluted” (LRT < 25<sup>th</sup> percentile). The difference between these two categories is a measure of the net Asian enhancement above the background and reaches a maximum in the spring of 30 ppbv CO and in the spring-fall of 7 ppbv O<sub>3</sub>. The Asian O<sub>3</sub> enhancement peaked at an average of 4 ppbv from April to October, which is the time of year of greatest urban air quality concerns in North America. Numerous long-range transport “events” (defined by at least 24 continuous hours of LRT > 75% percentile) were observed throughout the year. Ozone behavior was quite complicated during these events, producing no consistent enhancements. Classification of the measurements with LRT values from GEOS-CHEM is compared to back trajectories – both isentropic and kinematic. Isentropic trajectories agree reasonably well with GEOS-CHEM between February and May in capturing the CO

enhancements in air masses influenced by recent emissions, but were found to be less useful from June – January. Hysplit kinematic trajectories were slightly better at capturing the Asian pollution events than isentropic, but still missed an event during the summer completely that was verified by GEOS-CHEM. Possible reasons for poor trajectory performance in the summer and fall are discussed. Long-range transport appears not to affect the magnitude of the diurnal variability of O<sub>3</sub> measurements at CPO, which reflect daytime production of 2-4 ppbv/day. Rather, ship traffic in the vicinity of CPO, which supplies NO<sub>x</sub> through combustion, likely plays a dominant role.

## **1. Introduction**

Long-range transport of ozone (O<sub>3</sub>) and its precursors is a central issue to understanding the dispersion of anthropogenic pollution and the global perturbation of tropospheric photochemistry. O<sub>3</sub> is a significant pollutant at the surface because it is linked to health effects and vegetation damage at concentrations not far above ambient in most urban areas. Of particular concern is the background contribution to the local O<sub>3</sub> burden. Typical values of O<sub>3</sub> in the remote northern hemisphere range between 20-50 ppbv, depending on season and altitude [Oltmans and Levy II, 1994]. Recent model estimates have suggested that in the summer as much as 7 ppbv of the North American O<sub>3</sub> burden comes from Asian and European fuel combustion [Fiore *et al.*, 2002]. Likewise, North American anthropogenic emissions are estimated to contribute up to 10 ppbv to European O<sub>3</sub> during the summer [Li *et al.*, 2002; Langmann *et al.*, 2003], which may have caused 20% of the violations of the European Council ozone standard (55 ppbv, 8-hr average) in 1997 [Li *et al.*, 2002]. Estimates of the European influence on background O<sub>3</sub> in Asia suggest a 1-3 ppbv contribution of O<sub>3</sub> from transcontinental

transport [*Pochanart et al.*, 2003]. These examples point to the challenges in the effective design of air pollution control strategies for regions that are currently having difficulty with attainment.

Estimates of the future economic growth in the East Asian region point to a dramatic increase in fossil fuel combustion. By 2020, China is expected to have a 2-4-fold increase in NO<sub>x</sub> emissions (from 1990 levels) due to rapid development of the transportation sector [*Elliot et al.*, 1997; *Streets and Wahldoff*, 2000]. This will likely increase the amount of O<sub>3</sub> exported to North America [*Jacob et al.*, 1999; *Yienger et al.*, 2000]. Numerous episodes of pollution of Asian origin have already been measured in the North Pacific and on the west coast of North America [*Jaffe et al.*, 1998; 1999; 2001; 2003a; *Kotchenruther et al.*, 2001a; *Price et al.*, 2003; *Jaeglé et al.*, 2003]. However, to what extent these episodes control the background seasonality of O<sub>3</sub> and other pollutants like carbon monoxide (CO) in the boundary layer is still unclear. In addition to episodes, there is also evidence that springtime background O<sub>3</sub> concentrations have risen by 30% over western North America since the 1980s [*Jaffe et al.*, 2003b].

Most previous measurements of O<sub>3</sub> and its precursors in the northeastern Pacific have only been made in the springtime (March-May) in part because of a higher probability of seeing long-range transport compared to other seasons [*Jaffe et al.*, 1999; 2001; *Newell and Evans*, 2000; *Kotchenruther et al.*, 2001a; *Staudt et al.*, 2001; *Price et al.*, 2003; *Jaeglé et al.*, 2003; *Huebert et al.*, 2003; *Fuelberg et al.*, 2003]. This stems from relatively long lifetimes of O<sub>3</sub> and related species during spring and an increase in frontal activity in East Asia, whereby pollutants are lifted from the boundary layer for transport in the free troposphere [*Bey et al.*, 2001a; *Liu et al.*, 2003; *Jaeglé et al.*, 2003]. In contrast, very little is known about trans-Pacific transport processes in other seasons. Summer in particular is when many populated regions in the U.S.

have difficulty meeting the national ozone standard (84 ppbv, 8-hr average). Even a small increase from long-range transport would make attainment more difficult [*Jacob et al.*, 1999].

In this study, we use CO and O<sub>3</sub> measurements from Cheeka Peak Observatory (CPO) and results from the GEOS-CHEM global chemical transport model to quantify the effect of Asian and European anthropogenic emissions on a relatively cleaner background. We present a comparison of GEOS-CHEM vs. two types of back trajectories in their abilities to segregate air masses into cleaner and more polluted categories and to capture significant long-range transport events. Diurnal cycles of O<sub>3</sub> are also observed during the spring and summer and their relationship to ship emissions in the region is discussed.

## **2.0 Methods**

Measurements of CO and O<sub>3</sub> were conducted at Cheeka Peak Observatory (CPO) on the northwestern tip of the continental U. S. (48.3°N, 124.6°W, 480 m above sea level, see map in Figure 1). The site is on a ridge-top approximately 5-km inland of the Pacific Ocean in a very remote area with minimal sources of pollution in the immediate surroundings. CPO consistently lies in the marine boundary layer and during periods of westerly flow, there is little influence from recent North American emissions. Ocean-going ships, however, have a sporadic influence on the concentrations of NO<sub>x</sub> and aerosols at the site, but do not appreciably affect CO [*Jaffe et al.*, 2001]. The climate is marine temperate with over 200 cm of rainfall a year, about 80% of which falls between November and April. During periods of easterly flow, the site receives polluted air from the populated Vancouver-Seattle-Portland corridor. These periods are easily detectable by increases in CO, particle scattering, radon, and other continental tracers [*Weiss-Penzias et al.*, 2003]. The site has been used for atmospheric chemistry and aerosol research for

nearly 20 years [*Anderson et al.*, 1999]. The data used in this paper were collected from March 2001 to May 2002 (PHOBEA-II). In addition, we use data from March and April of 1997 and 1998 (PHOBEA-I, previously reported by *Jaffe et al.*, 1999; 2001). The period of March – May 2002 corresponded with the Intercontinental Transport and Chemical Transformation 2002 (ITCT 2K2) campaign [*Parrish et al.*, this issue].

CO and O<sub>3</sub> were measured using the same methods as previous campaigns [*Jaffe et al.*, 2001]. Briefly, both species were measured from a common inlet situated atop a 10 m tower. The gases were sampled through 15 m of ¼” OD Teflon tubing. The sample stream was teed with one side going to a non-dispersive infrared CO instrument (API-300, Advanced Pollution Instruments, San Diego, CA) and the other going to a standard UV absorbance O<sub>3</sub> analyzer (Dasibi 1008 RS). The CO instrument was modified to reduce water vapor interference and improve detection limits [*Jaffe et al.*, 1998]. The CO instrument was calibrated daily using a NIST traceable standard and the O<sub>3</sub> instrument was calibrated quarterly using an ozone generator (Columbia Scientific), which was calibrated against a Washington Department of Ecology primary standard. In 2001, another Dasibi O<sub>3</sub> instrument from our lab was used as a transfer standard to check the accuracy of our O<sub>3</sub> calibrations. The precision of the CO and O<sub>3</sub> instruments was similar to that reported previously [*Jaffe et al.*, 2001] at 9% and 2%, respectively for an hourly average. The accuracy of these measurements over the 6-year period spanning the data set, due to calibration errors and standard drifts is estimated to be better than 5%.

Similar to our previous analyses [*Jaffe et al.*, 1999; 2001; *Kotchenruther et al.*, 2001a] isentropic 10-day back trajectories were calculated for CPO at 0 and 12 GMT for each day of the measurement periods [*Harris and Kahl*, 1994], using the Level III-B Basic Consolidated Dataset

from the European Centre for Medium-Range Weather Forecasts (ECMWF). These meteorological fields have a 6-hour time resolution, and a horizontal resolution of  $2.5^{\circ}$  latitude x  $2.5^{\circ}$  longitude with 23 vertical layers. We also used 10-day back trajectories from the HYSPLIT\_4 model (Hybrid Single-Particle Lagrangian Integrated Trajectory, hereafter referred to as Hysplit kinematic trajectories) [Hysplit, 1997] during selected long-range transport events as an accuracy check against isentropic trajectories. The Hysplit kinematic trajectory model was operated with the National Center for Environmental Prediction's (NCEP) FNL meteorological data set, which has a time resolution of 6-hours, and a horizontal resolution of 191 km with 13 vertical layers. These trajectories were also calculated at 0 and 12 GMT.

While there are known problems with assumptions associated with the isentropic approach (such as near the surface and in the presence of precipitation) [Stohl *et al.*, 1998 and references therein], there are numerous examples in the literature where it has been used successfully for chemical transport analyses [Merrill, 1994; Moody *et al.*, 1995; Simmonds *et al.*, 1997; Harris *et al.*, 2000; Jaffe *et al.*, 2001]. The Hysplit kinematic approach uses the 3-dimensional wind components to generate its trajectories, which have been observed to give more realistic vertical and horizontal displacements than the isentropic approach [Fuelberg *et al.*, 1996].

Trajectories arriving at CPO were classified in one of four ways (see map in Figure 1): those that crossed east of  $124^{\circ}\text{W}$  were called "local", those that crossed south of  $60^{\circ}\text{N}$  and west of  $150^{\circ}\text{E}$  were called "Asian", those that crossed south of  $35^{\circ}\text{N}$  were called "subtropical" (ST), and all other trajectories were called "North Pacific" (NP). The "Asian" region extends  $10^{\circ}$  further north than that used by Jaffe *et al.* [2001] since it has been recognized that Asian outflow shifts northward during the summer and fall [Liang *et al.*, this issue].

The GEOS-CHEM global chemical transport model was also used, which is a global three-dimensional model of tropospheric chemistry [Bey *et al.*, 2001b], driven by assimilated meteorological data for the specific years of this study, compiled at the Goddard Earth Observing System (GEOS) of the NASA Global Modeling and Assimilation Office (GMAO). The spatial resolution is  $2^\circ$  latitude x  $2.5^\circ$  longitude in the horizontal, with 30 vertical levels for the 2001/2002 runs and 26 vertical layers for the 1997/1998 runs. Surface meteorological fields have a 3-hour time resolution and upper-level fields have a 6-hour time resolution. In this work, we have used 6-hour averages from a CO-only simulation using archived monthly OH fields from a full chemistry run [Bey *et al.*, 2001a; Li *et al.*, 2002]. Modeled CO is “tagged” by its sources and regions, which include Asian, European, and North American fossil fuel, biofuel and biomass burning, as well as oxidation of methane, isoprene and other volatile organic compounds (VOCs) [Duncan *et al.*, 2003b]. This model has shown very good agreement with CO measurements from the “marine” and “continental” sectors at CPO using ground-based and vertical profile data from spring 2001 [Jaeglé *et al.*, 2003]. Further information about the GEOS-CHEM simulation used in this work is given in Liang *et al.* [this issue].

### **3.0 Results and Discussion**

#### **3.1 Measurements**

In this paper, we focus on the marine air masses at CPO, which were identified using locally measured wind directions (between  $160^\circ - 315^\circ$ ), wind speeds (greater than 2 m/s), and isentropic back trajectories that showed the air had not crossed east of  $124^\circ\text{W}$  [Jaffe *et al.*, 2001]. All model results were segregated in an identical fashion. In this paper, the terms “marine”, “marine-only”, and “background” are used interchangeably. Table 1 shows the number of hours

in each month that were classified as “marine”. These vary from a low of 282 hours (42%) in February to a high of 630 hours (85%) in July, with an annual average of 425 hours or 59% of the time. March, April, and May represent more than one-year’s worth of data but have been normalized to a monthly average. In general, winter and spring have less “marine” periods than the summer due to more frequent springtime surface high-pressure systems that produce low-level easterly flow. In addition, there are fewer storms during the summer months resulting in a more consistent on-shore flow.

The three sources of data used here have different time-scales (measurements = continuous hourly averages, GEOS-CHEM = 6 hour averages, and trajectories = every 12 hours). In comparing measurements with GEOS-CHEM, three hours of measurements before and after the time of the GEOS-CHEM data point were averaged. For comparison with trajectories, 6-hours of measurements before and after the time of the trajectory were averaged.

Table 1 and Figure 2A show the monthly means of our CO and O<sub>3</sub> measurements during the PHOBEA I-II campaigns. CO measurements from October 2001 have been omitted since there was a 3-week data gap due to instrument maintenance. The annual cycle of CO at CPO is similar to that of other northern hemisphere remote sites and consistent with the observed latitudinal gradient over the Pacific [Novelli *et al.*, 1992; 1998]. The spring maximum (March = 159 ppbv) and summer minimum (August = 78 ppbv) are primarily driven by the seasonal cycle in OH concentrations and the seasonality of transport processes [Holloway *et al.*, 2000]. Reaction with OH accounts for up to 95% of the global sink, which gives a CO lifetime of about one month in the summer and up to a year during the winter in the midlatitudes [Novelli *et al.*, 1998]. The North Pacific atmosphere is the most affected by direct Asian outflow of pollutants during the spring and the least affected during the summer [Jacob *et al.*, 2003]. This combined

effect of chemistry and transport causes about a factor of 2 drop in CO concentration from spring to summer.

The annual cycle of O<sub>3</sub> in Figure 2A also shows a spring maximum (April = 45.8 ppbv) and a summer minimum (July = 28.4 ppbv), and this general feature has been observed at other remote locations in the marine boundary layer (e.g. Mace Head, Ireland, and Bermuda) [*Oltmans and Levy II*, 1994]. Long-range transport from pollution sources and the seasonality in OH also play important roles in the seasonality of surface O<sub>3</sub>, producing a similarity to the CO cycle [*Parrish et al*, 1998]. The O<sub>3</sub> budget is also influenced by downward transport from the stratosphere [*Moody et al.*, 1995], dry-deposition to the sea-surface [*Lelieveld and Dentener*, 2000], loss in clouds via aqueous chemistry [*Barth et al.*, 2002] and destruction by halogen radicals associated with sea salt aerosols [*Dickerson et al.*, 1999]. O<sub>3</sub> at CPO differs slightly from other marine boundary layer (MBL) sites in that the spring maximum is much less pronounced, with O<sub>3</sub> levels changing by < 5 ppbv in the eight months between October and May, compared to about 10 ppbv for Mace Head and Bermuda over the same time period [*Oltmans and Levy II*, 1994]. Part of the reason for the smaller spring increase at CPO could be the great distance between CPO and pollution sources to the west, which would allow for more thorough dilution of pollution plumes. Additionally, frequent wintertime storms at CPO could enhance O<sub>3</sub> levels due to deep mixing with the upper troposphere during the passage of cold fronts [*Kunz and Speth*, 1997].

### **3.2 Comparison of CO Measurements with GEOS-CHEM**

Shown in Figure 2A is a comparison between monthly means of measured and modeled CO. The model captures the general features of the annual cycle of CO quite well, peaking in

March and reaching a minimum in August. The model shows a negative offset of about 8% from December – May, and a 10-15% positive offset from July –September, although the means generally fall within one standard deviation of one another. On an annual basis, the correlation between the model and measurements is quite strong ( $r = 0.92$ , using 6-hour averages), primarily because GEOS-CHEM captures the seasonal cycle of CO, which drives the correlation. The average of each monthly correlation, shown in Table 1, is 0.53, with winter/spring providing the strongest correlations ( $r = 0.50$  to  $0.79$ ) compared to summer/fall ( $r = 0.16$  to  $0.60$ ). An overestimation of isoprene emissions in the model has been used to explain the poorer model performance in summer/fall at CPO [*Liang et al.*, this issue; *Abbot et al.*, 2003].

Figure 2B shows the breakdown of CO sources (medians) in GEOS-CHEM: “LRT” (combination of Asian biomass burning, and Asian + European fossil-fuel and biofuel combustion), “Oxidation-CO” (oxidation of methane and biogenic VOCs), and “NA” (fossil fuel combustion from North America). LRT is the dominant source of CO at CPO between January and May, with a maximum of 76 ppbv (49%) in April. This arises from the relatively longer lifetime of CO in the winter/spring in conjunction with the dominance of westerly flow and entrainment of Asian emissions throughout the midlatitudes [*Jacob et al.*, 2003]. Asian biomass burning (included as part of LRT) is a minor contributor to total CO, comprising less than 6 ppbv (7%) at its maximum during the spring. Biomass burning CO emissions in the model include interannual variability for the 1997 and 1998 simulations, and are based on seasonally varying climatological values developed by *Duncan et al.* [2003] for the 2001 and 2002 simulations. Thus, the model does not account for periodic strong enhancements of Siberian biomass emissions, as seen recently in the free troposphere by *Bertschi et al.* [this issue] during the spring of 2002 and at the surface during the summer of 2003 [*Jaffe*, unpublished data]. “Oxidation-CO”

dominates from July – October, reaching a peak of 50 ppbv (56%) in August. The seasonality of Oxidation-CO is largely a function of OH, in addition to the increase in biogenic emissions of isoprene during the northern hemisphere growing season. NA represents CO that has undergone circumpolar transport and arrives at CPO from the west, since the data set has been screened to eliminate direct easterly transport to the site. NA reaches its peak in the winter/spring at 22 ppbv (15%) of the total in February, primarily due to the longer lifetime of CO in the winter.

### **3.3 Using LRT from GEOS-CHEM to Segregate CO and Ozone Measurements**

In this section, we investigate the degree to which measured CO at CPO can be explained by the LRT parameter. Table 2 shows the monthly correlation coefficients ( $r$ ) between these two quantities, giving a monthly average of  $r = 0.60$ . As with total modeled CO, the strongest correlations occur between January and August. This points to the importance of LRT in controlling the variability of CO during this part of the year. Later in the fall, CO-LRT correlations weaken largely because the model then attributes lower importance to LRT.

For each month, we have used the distribution of LRT values as a segregation tool for CO and O<sub>3</sub> observations. 75<sup>th</sup> and 25<sup>th</sup> percentile values of LRT have been somewhat arbitrarily selected for identifying time periods of relatively “polluted” or “clean” air from the marine sector, respectively. This is analogous to data segregation using back trajectories [e.g. *Simmonds et al.*, 1997; *Derwent et al.*, 1998; *Jaffe et al.*, 1999; 2001] to identify distinct source regions, based on the likely path of an air mass before measurement. However, segregating the data based on LRT > 75% and LRT < 25% criteria incorporates mixing, chemical processing, and emission strengths in addition to the geographical origin of an air mass. As will be shown

below, this produces a better agreement with the measurements compared to using either the isentropic or Hysplit kinematic trajectories.

The strength of the segregation between polluted and clean categories – how distinct these categories are from one another – is indicated by the variability of LRT in a given month. This variability can be seen in the monthly probability distribution of LRT values, shown in Figure 3. The medians of these distributions correspond to the LRT values presented in Figure 2B. The median, 75<sup>th</sup> percentile, and 25<sup>th</sup> percentile LRT values are shown in Table 2. The difference between the 75<sup>th</sup> percentile and 25<sup>th</sup> percentile values reaches a maximum in May (17 ppbv) and a minimum in July and September (5 ppbv). May variability is largely caused by the seasonal cycle of CO, which results in a dramatic drop in LRT values from the first to the last parts of May. On a seasonal basis, LRT > 75% - LRT < 25% values display the highest variability from February – June (11-17 ppbv) compared to July – January (5-8 ppbv). This higher variability in the spring is consistent with the seasonality of meteorological patterns over the Pacific, which favor more rapid transport followed by relatively quiescent periods [*Yienger et al.*, 2000; *Liu et al.*, 2003; *Jacob et al.*, 2003]. In addition to these “episodes”, however, we also point out that so-called “clean” conditions at CPO, particularly in the spring, do not exist. Figure 3 shows that LRT during March and April is rarely less than 50 ppbv (about one-third of the total CO).

During months with very low LRT variability (July – January), our “cleaner” and “more-polluted” categories are only weakly separated, and approach the uncertainty of the CO measurements (9% uncertainty in an hourly average, or 4% in a 6-hour average). Thus, based on LRT values alone, we can only tentatively assign the measurements to different categories in the months where LRT is low and/or less variable. However, in spite of these limitations, we are

able to identify some specific events consistent with the observations, which are largely missed using trajectory classifications alone.

The results of segregating CO and O<sub>3</sub> measurements using LRT > 75% and LRT < 25% are shown in Figure 4, along with all marine data. The upper panel (4A) shows that LRT > 75% CO measurements (CO<sub>LRT75</sub>) are higher in every month than LRT < 25% measurements (CO<sub>LRT25</sub>), providing a reasonable measure of validation to our method. The difference between these two classifications can be seen in the inset of Figure 4B, reaching a peak of 30 ppbv in April. This is a measure of the Asian enhancement above the background. The January – June enhancement (23 ppbv) is significantly higher than that for July – December (10 ppbv), consistent with the model results (Table 2). This indicates that the first part of the year, and particularly during April, variability in long-range transport plays a larger role in controlling CO concentrations at CPO than later in the year.

Figure 4B shows the data segregation results for O<sub>3</sub>. Here the difference between O<sub>3LRT75</sub> and O<sub>3LRT25</sub> reveals a different seasonality compared to CO. The peak for O<sub>3</sub> occurs in April and September at nearly 7 ppbv, with the 6-month period of Apr. – Oct. showing the greatest average difference (4.4 ppbv) compared to Nov. – Mar. (0.0 ppbv). This shows that while long-range transport of CO is strongest in winter/spring, O<sub>3</sub> from distant sources has its maximum influence much later in the year, coinciding with the summer smog season in urban areas of North America, as suggested by Jacob et al [1999]. October – December, and February show no apparent Asian contribution of O<sub>3</sub>, even though the East Asian region is thought to be a net exporter of O<sub>3</sub> to the Pacific in all seasons [Mauzerall et al., 2000]. This could be explained by urban titration of O<sub>3</sub> by NO<sub>x</sub> in Asia, similar to the observations of Parrish et al. [1998] downwind of the Eastern U.S. However, O<sub>3</sub> loss in transit due to very low NO<sub>x</sub> levels may also

be important, combined with negligible O<sub>3</sub> production due to low in-situ temperatures and light levels.

### **3.4 Using GEOS-CHEM to Identify Long-Range Transport Events**

There have been numerous observations of events at CPO and over the eastern Pacific [Jaffe *et al.*, 1999; 2001; Kotchenruther *et al.*, 2001; Fuelberg *et al.*, 2003; Huebert *et al.*, 2003; Price *et al.*, 2003; Jaeglé *et al.*, 2003]. Here we use GEOS-CHEM results and our CO observations to identify events during all seasons at CPO, not just in spring, as has previously been the case. An event was determined if the following criteria were met: 1) model-generated LRT values reached > 75<sup>th</sup> percentile for at least 24 hours continuously, 2) total modeled CO and measured CO were enhanced by a statistically significant ( $P > 0.95$ ) amount above their respective monthly means, and 3) measured vs. modeled CO correlations ( $r$ ) were > 0.10. The duration of an event was identified in two ways: the total number of hours when LRT > 75%, and the time between LRT minima on both sides of the LRT maximum. This latter criterion was used for calculating  $\Delta\text{CO}$  and  $\Delta\text{O}_3$  values, along with correlation coefficients. Table 3 shows a list of all events identified from our data set using these criteria.  $\Delta\text{CO}$  refers to the difference between the event maximum (6-hr average) and the monthly mean.  $\Delta\text{O}_3$  is the difference between the measured O<sub>3</sub> value at the time of the measured CO event maximum, and the monthly O<sub>3</sub> mean. There is good agreement between total modeled and measured CO during the events as shown by the correlation coefficients in Table 3. Table 4 shows a list of events that met the first criteria but not both (2) and (3), and will be discussed below. The date of each event refers to the approximate midpoint (GMT).

Table 3 has been shaded to indicate the season of each event, showing that there are 3-4 events in spring, 2 events in summer, 2 events in fall, and 3 events in winter. There is no clear seasonal trend in the duration of events, with times ranging from 24-78 hours of LRT > 75%. However, there is a seasonal trend in the magnitude or strength of these events, as shown by the lack of an event with  $\Delta\text{CO}_{\text{meas.}} > 20$  ppbv during the summer and fall. This is consistent with our view of winter and spring as being more influenced by long-range transport, and summer/fall being a more quiescent period. A number of events seen here have been reported elsewhere: 29-Mar-97 [Jaffe *et al.*, 1999], 11-Mar-01 [Jaeglé *et al.*, 2003], 20-Jan-01, 27-Mar-02, and 15-May-02 [Liang, *et al.*, this issue; Price *et al.*, this issue].

Table 3 shows that O<sub>3</sub> is not significantly enhanced, taking the time-weighted average of all events. It also does not appear to follow any particular seasonal trend, which is somewhat confusing. Based on our GEOS-CHEM segregation results in Figure 4A, we would expect late spring/summer events to bring enhanced O<sub>3</sub>. However, the two events in July both brought a drop in O<sub>3</sub> concentrations, and a negative O<sub>3</sub>-CO correlation. The event on 15-May-02 brought the largest O<sub>3</sub> decrease of any event (-6.4 ppbv). Large O<sub>3</sub> enhancements (> 4 ppbv) also occur in some events, restricted to spring and winter. The high degree of O<sub>3</sub>-CO correlation for all events taken together is a function of the similarity in the O<sub>3</sub> and CO seasonal cycles, rather than many individual events having strongly positive correlations. As has been noted previously, air masses with clear anthropogenic signatures do not always contain O<sub>3</sub> enhancements [Jaffe *et al.*, 2003]. O<sub>3</sub> behavior can be complicated by the presence of mineral dust [He and Carmichael, 1999], destruction during transit over the ocean, or the possible mixing with stratospheric O<sub>3</sub> [Carmichael *et al.*, 1998]. In fact, the 29-Apr-01 and 9-Jan-02 events showed relatively large O<sub>3</sub>

increases and were associated with dry air and relatively small CO increases, which suggests a possible stratospheric influence.

Three events in both spring and summer were predicted by GEOS-CHEM, but did not produce a good correlation with the measurements and/or did not result in a significant increase in measured CO. These are listed in Table 4. In most cases, GEOS-CHEM accurately predicted the presence of enhanced pollution, but missed the exact timing of the event, leading to an insignificant or even negative correlation. Only in two cases, did GEOS-CHEM appear to predict an event that was not observed at all (20-Mar-97 and 4-Aug-01). The 23-Apr-02 case has been reported by *Liang et al.* [this issue] and is an example of a time when measured CO peaked and dropped rapidly about 24 hours before the maximum in LRT and total modeled CO. This resulted in a correlation of  $r = -0.75$ , even though the magnitude of the observed CO increase agrees very well with the model.

### **3.5 Comparison of GEOS-CHEM with Back Trajectories**

In this section we compare isentropic and Hysplit kinematic trajectories with GEOS-CHEM; both in their ability to accurately segregate CO/O<sub>3</sub> measurements into cleaner and more polluted categories and to capture individual events. Isentropic trajectories were calculated every 12 hours throughout the entire time period of the measurements and Hysplit kinematic trajectories were calculated during selected events for the purposes of checking the accuracy of the simpler isentropic model. In comparing trajectories to GEOS-CHEM, LRT > 75% from the previous sections is analogous to “Asian” trajectories and LRT < 25% is analogous to “subtropical” trajectories, as defined in section 2.0. Part of the motivation for such a comparison is that some of our current and past work has relied upon using both isentropic and Hysplit

kinematic back trajectories [*Price et al.*, this issue; *Bertschi et al.*, this issue; *Kotchenruther et al.*, 2001a; *Jaffe et al.*, 1999; 2001] and we wish to assess their performance relative to a global chemical tracer model. However, it should be noted that air mass pathways from GEOS-CHEM might be quite different from those obtained from trajectories – merely due to the different types of meteorological data being used as inputs to each model. Each data set has a different spatial and temporal resolution, which may lead to different conclusions about the degree of Asian influence [*Pickering et al.*, 1996; *Fuelberg et al.*, 1996]. Thus, even though we feel that the following comparison between GEOS-CHEM and trajectories shows a general limitation of trajectories for this type of analysis, we must keep in mind that our results could be sensitive to model input parameters.

In Figure 5 we present the results from an isentropic trajectory segregation of the monthly averaged CO and O<sub>3</sub> measurements, where the format is identical to Figure 4. At first glance, isentropic trajectory segregation produces some of the same results as those obtained with GEOS-CHEM. The inset of Figure 5A shows that Asian-CO is larger than ST-CO in most months, especially spring, where the difference reaches ~20 ppbv, which is comparable in timing and magnitude to the difference between CO<sub>LRT75</sub> and CO<sub>LRT25</sub> in Figure 4A. The Asian-O<sub>3</sub>/ST-O<sub>3</sub> difference (Figure 5B) shows a spring maximum as well, which is in agreement with O<sub>3</sub><sub>LRT75</sub> and O<sub>3</sub><sub>LRT25</sub>. The magnitude of the maximum Asian influence for O<sub>3</sub> is also comparable to that in Figure 4B (~5 ppbv). Springtime Asian pollution events are also fairly well captured by isentropic trajectories. We found that 56% of the total LRT > 75% hours during spring events corresponded to an Asian classification (Table 5). During March and April, isentropic trajectories captured 70% of the events. These demonstrated similarities to GEOS-CHEM in the

spring give a measure of confidence to past studies at CPO that relied solely upon isentropic trajectories [Jaffe et al., 1999; 2001; Kotchenruther et al., 2001a].

However, in contrast with GEOS-CHEM, isentropic trajectories do not provide much meaningful information from June – January. In particular, on Table 6 we see that from June – September, only one “Asian” isentropic trajectory was identified. To ascertain whether this lack of isentropic trajectories was due to a limitation associated with the isentropic model, we also calculated Hysplit kinematic trajectories for the Asian events as shown in Table 3. This comparison between Hysplit kinematic, isentropic, and GEOS-CHEM during these events is shown in Table 5. Here we see that both Hysplit kinematic and isentropic trajectories classify many fewer hours as “Asian” than GEOS-CHEM in summer (12-24%) and fall-winter (33-48%). While Hysplit kinematic generally captures more of each Asian pollution event and misses fewer events completely, it does not appear to be dramatically better than isentropic trajectories.

One explanation for the limitation of trajectories between June – September could be that we limit the trajectories to 10-days back in time, due to excessive errors that can arise when trajectories are calculated for longer periods. Since winds are generally lighter over the Pacific in the summer and fall compared to the winter and spring, [Liang et al., this issue], transport from the Asian continent can take longer than 10 days, thus preventing trajectories from classifying an air mass as “Asian”. Hysplit kinematic back trajectories from 3 events in the summer and early fall (12-Jul-01, 16-Jul-01, 28-Sep-01) were inspected for this phenomenon. Trajectories from 12-Jul-01 (LRT > 75% = 48 hrs) showed that air masses originated over the North Pole and Alaska, suggesting that the 10-day trajectory limit was not an issue for this event. Likewise, trajectories from 28-Sep-01 (LRT > 75% = 78 hrs) did not cross east of 160°W after 10-days and originated mainly from Alaska. Trajectories from the 16-Jul-01 event (LRT > 75%

= 54 hrs), however, terminated in the North Pacific around 170°E, suggesting that had we been able to follow the air mass back more than 10-days, it may have originated over Asia. Thus, while it seems that slower transport may put 10-day trajectories at a disadvantage compared with GEOS-CHEM, this effect does not explain all of events that were missed by trajectories.

In addition to the lack of “Asian” trajectories between June – September, there appear to be several misclassified “Asian” isentropic trajectories throughout the year. This leads to the result shown in Figure 5A, where Asian-CO is actually smaller than ST-CO in November and December. To verify that this is caused by misclassified “Asian” trajectories and not misclassified “ST” trajectories, we compared the “Asian” time periods to the GEOS-CHEM results and CO measurements for each month. This is shown in Table 6, where “Asian” isentropic trajectories are grouped into “agreement” and “disagreement” categories, based on whether they corresponded to  $LRT > 75\%$  or  $LRT < 25\%$  classifications, respectively. The most disagreement occurred in November, with one-half (48 out of 96) the total “Asian” hours corresponding to  $LRT < 25\%$ . The average measured CO concentration during these times was 11 ppbv less than the marine mean, suggesting that Asian pollution events were not occurring when “Asian” isentropic trajectories were being classified, in agreement with GEOS-CHEM. Only 24 out of 96 hours were classified as “Asian” & “ $LRT > 75\%$ ” in November, thus explaining why Asian-CO was about 10 ppbv lower than ST-CO, shown in the inset of Figure 5A. December, February, March and April also had some occurrences of “Asian” & “ $LRT < 25\%$ ”, although less than November. In each case, the measured CO value is much less than the monthly mean, suggesting a misclassification. In contrast, during times of agreement between isentropic trajectories and GEOS-CHEM (“Asian” & “ $LRT > 75\%$ ”), measured CO is nearly always above the means. Some of the disagreement periods gave trajectories that originated at

altitudes higher than 2 km over Asia, raising the possibility that the air masses were effectively isolated from the surface emissions. It would seem that this type of trajectory, a so-called “clean Asian”, is more likely to occur in the fall and winter.

In addition to seasonal/monthly differences between GEOS-CHEM and trajectories, a series of events from April-May 2001 shows important short-term inconsistencies as well. Figure 6 shows the time-series measurements of CO and O<sub>3</sub>, model-calculated LRT, Oxidation CO, and NA from GEOS-CHEM, and isentropic and Hysplit trajectory classifications. These data have not been segregated by the “marine-only” criteria. One difference shown is in the classification of locally influenced air. GEOS-CHEM predicts two small, but significant peaks in NA (events “a” and “d” in Figure 7), which are reflected in the measurements (both CO and O<sub>3</sub> show increases). Isentropic trajectories classified these periods as “subtropical” and “North Pacific”, and Hysplit classified them as “local” and “North Pacific”. For both these events, Hysplit and isentropic trajectories showed that the backward path of the air masses stayed close to 124°W (the “local” boundary), came up from the south and probably picked up pollutants from Portland, Oregon and other smaller coastal cities.

Events “b” and “c” compare the abilities of GEOS-CHEM and trajectories to classify periods of long-range transport. During event “b”, the measured CO rise corresponds to a peak in LRT. Hysplit classifies this time as “Asian”, whereas isentropic trajectories do not. In event “c”, both trajectory models predict an Asian influence, while LRT and the CO measurements show significant decreases here. GEOS-CHEM more accurately (though not perfectly) captures this event.

### **3.6 Correlations Between O<sub>3</sub> and CO**

The degree of correlation between O<sub>3</sub> and CO can give information on the extent to which O<sub>3</sub> is being photochemically produced from primary pollutants that are co-emitted with CO [Chin *et al.*, 1994; Atherton *et al.*, 1996; Parrish *et al.*, 1998; Mauzerall *et al.*, 2000;]. The slope obtained from an O<sub>3</sub>-CO plot is related to the photochemical production efficiency of O<sub>3</sub> in the pollution plume, and the length of time since pollution emissions. Values of 0.3 – 0.4 O<sub>3</sub> ppbv/CO ppbv are typical for air masses recently influenced by industrial emissions [Chin *et al.*, 1994; Parrish *et al.*, 1998]. Price *et al.* [this issue] observed lower values during the spring at CPO, where dilution and other processes affecting O<sub>3</sub> have more time to occur. In Figure 7 we show the O<sub>3</sub>-CO slopes (“marine-only” data) as a function of the square of the correlation coefficient ( $r^2$ ) at CPO for the entire year. The general pattern of this plot is roughly in the shape of the letter “C”, where April – September produce the largest positive correlations, January – March are only slightly positive, and October – December show slight negative correlations. This is consistent with the results shown in Figure 4, where O<sub>3</sub> and CO are both enhanced during periods of LRT > 75% in the spring and summer, whereas CO is enhanced and O<sub>3</sub> is lowered during November and December. This seasonal correlation pattern is analogous to that of Parrish *et al.* [1998], although their data from Sable Is., Canada produced much greater correlations, both positive and negative, due to closer proximity to pollution sources.

### 3.7 *Diurnal Cycles of O<sub>3</sub>*

O<sub>3</sub> concentrations from “marine-only” data averaged by local time of day for each two-month period during the year are shown in Figure 8. May - June, and September - October are shown as individual months since seasonal changes in O<sub>3</sub> during these times of the year can overwhelm any diurnal variability. Diurnal cycles of CO are not discernible above background

variations in any season and are not shown. Notice the consistent O<sub>3</sub> diurnal patterns in the plots covering March through August, which show a rise of about 2-4 ppbv during the sunlit hours (8:00 AM – 8:00 PM). Diurnal land-sea breezes are not a factor since all data have been segregated by wind direction. These diurnal patterns are consistent with net photochemical production, which would require a local source of NO<sub>x</sub>. The amount of NO<sub>x</sub> needed to generate our observed O<sub>3</sub> production rate of 2-4 ppbv/day is on the order of 100-250 pptv [Liu *et al.*, 1987; Herring *et al.*, 1997]. Measurements of NO<sub>x</sub> at CPO by Jaffe *et al.* [2001] show a March-April average of 189 pptv of NO<sub>x</sub>, but with high variability, consistent with the range required to produce our observed daily production of O<sub>3</sub>. Jaffe *et al.* [2001] highlight the importance of ocean-going ships in controlling NO<sub>x</sub> levels at CPO (due to the close proximity of the Straits of Juan de Fuca). Ships may also be an important influence on the NO<sub>x</sub> budget of the remote MBL [Crutzen and Lawrence, 1999], which should be largely independent of season since shipping occurs throughout the year. Thus, O<sub>3</sub> production at CPO would mainly depend on available sunlight, being highest in the summer, lowest in the winter. Our results in Figure 8 are fairly consistent with this hypothesis; O<sub>3</sub> daily production is limited to the months with the greatest amount of sunlight, highest temperatures, and the least amount of cloud cover. The only exception is September and October, which show no apparent pattern. Thus, in these months, there are evidently other processes interfering with daily production of O<sub>3</sub>, even though climatologically, September and October provide as much sunlight as during the spring. One explanation is that peroxyacetyl nitrate (PAN) from long-range transport is a significant source of NO<sub>x</sub> in the spring but not in the fall [Kotchenruther *et al.*, 2001b].

However, an LRT-segregation of the data does not appear to influence the diurnal variability of O<sub>3</sub> at CPO. This can be seen in the March-April panel of Figure 8, which compares

the diurnal cycles from all marine, LRT > 75% and LRT < 25% segregated data. For simplicity, only the results from March-April are shown, although the data from other months is similar. Since the magnitude and phase of the diurnal cycles from both LRT categories is comparable, this again points to a local source of NO<sub>x</sub> (i.e. ships) as the dominant factor for the net O<sub>3</sub> production that we observe. Although there is much debate currently over the degree to which ship emissions influence the relatively pristine MBL [Song et al, 2003, and references therein], our previous data [Jaffe et al., 2001] suggest that CPO is under that influence. Thus, future O<sub>3</sub> measurements at CPO during the spring and summer should be viewed with this influence in mind.

#### **4.0 Conclusions**

In this work, CO and O<sub>3</sub> concentrations were analyzed, along with results from the GEOS-CHEM global chemical transport model and two types of back trajectories. The data from a full annual cycle allow us to determine the influence of long-range transported pollution on the seasonality of CO and O<sub>3</sub>. Using GEOS-CHEM, a quantity called “LRT” is obtained, which represents the amount of CO produced from Asian biomass burning, and Asian + European fossil- and bio-fuel sources. LRT correlates well with measured CO and thus, allows for segregation of the CO and O<sub>3</sub> data into “more polluted” and “less polluted” categories (> 75<sup>th</sup> percentile and < 25<sup>th</sup> percentile, respectively, of each month’s worth of LRT data). The difference in measured CO and O<sub>3</sub> between these two categories gives a measure of the net Asian enhancement above the background, which shows a maximum for CO (23 ppbv) during January – June and a maximum for O<sub>3</sub> (4.4 ppbv) during April – October. This shift in the timing of the O<sub>3</sub> maximum suggests that while long-range transport of pollutants is strongest

early in the year, maximum O<sub>3</sub> enhancement comes later, which may reflect changing O<sub>3</sub> production rates at the source regions.

The LRT parameter from GEOS-CHEM was used to identify specific long-range transport events at CPO. Criteria consisted of at least 24-hours of LRT > 75<sup>th</sup> percentile during the event, a positive model-measurement CO correlation and a statistically significant increase (P>0.95) in measured and total modeled CO. Events occurred throughout the year, with the strongest ones in winter and spring (measured CO enhanced > 20 ppbv above the mean). The time-weighted average enhancement for all 16 events is 16 ppbv for CO and 0.4 ppbv for O<sub>3</sub>. The predicted enhancement of total modeled CO is 17 ppbv, indicating that on average, the model does an excellent job of quantifying these events. O<sub>3</sub> behavior appeared complicated, with no apparent pattern of enhancement in any season. Some events with enhanced CO also had large O<sub>3</sub> enhancements, and were associated with dry air intrusions, suggesting a stratospheric influence on O<sub>3</sub> levels. Another 6 events were predicted by GEOS-CHEM, but did not show good agreement with the observations. In most of these cases, GEOS-CHEM accurately predicted the magnitude of the CO enhancements, but missed the timing of the CO maximum, thus leading to a poor measurement-model correlation.

The ability of LRT to classify CO/O<sub>3</sub> measurements is compared with both isentropic and Hysplit modeled vertical velocity back trajectories. The methods generally agree during the spring, in terms of the magnitude of enhancement from the “more polluted” vs. the “less polluted” categories (20-30 ppbv for CO and 0-6 ppbv for O<sub>3</sub>). However, important differences in all seasons were also highlighted. In particular, summer trajectories provided little information because only one “Asian” isentropic trajectory was classified between June and September. Both Hysplit kinematic and isentropic trajectories completely missed an “Asian”

pollution event, which occurred around 12-Jul-01. GEOS-CHEM was able to segregate the summertime measurements with some accuracy, showing a significant distant pollution influence on O<sub>3</sub>. During the fall, there were several “Asian” trajectories with levels of CO below the background, which were accurately predicted by GEOS-CHEM. Furthermore, during a particular spring period, GEOS-CHEM displayed better spatial and temporal resolution than trajectories by identifying periods of local and Asian influence when trajectories classified the air masses as the marine background.

Correlations between measured O<sub>3</sub> and CO, which are used as a measure of the relative quantity of O<sub>3</sub> produced from anthropogenic emissions, are generally weak throughout the year reflecting the mixing with cleaner source regions and the complex chemistry of O<sub>3</sub>. However, April – August show the strongest correlations,  $r^2 = 0.2 - 0.4$ ,  $\Delta O_3/\Delta CO = 0.2 - 0.3$ , which is consistent with the GEOS-CHEM results.

Finally, diurnal cycles of O<sub>3</sub> during the spring and summer show a consistent concentration increase during the daytime, suggesting photochemical production. NO<sub>x</sub> values measured in the spring are high enough to produce O<sub>3</sub> at the observed rates (2-4 ppbv/day). This NO<sub>x</sub> presumably comes from ships that enter and exit the Straits of Juan de Fuca. Diurnal patterns from LRT > 75% and LRT > 25% segregated data have the same phase and magnitude, which is consistent with this hypothesis.

Acknowledgements. This work was supported by the National Science Foundation. We thank the Makah Nation for allowing us to sample the atmosphere on their lands. James Dennison constructed the map used in this paper. The GEOS-CHEM model is managed by the

Atmospheric Chemistry Modeling Group at Harvard University with support from the NASA  
Atmospheric Chemistry Modeling and Analysis Program.

## Literature Cited

- Abbot, D. S., P. I. Palmer, R. V. Martin, K. V. Chance, D. J. Jacob, and A. Guenther, Seasonal and interannual variability of North American isoprene emissions as determined by formaldehyde column measurements from space, *Geophys. Res. Lett.*, *30*(17), 1886, doi:10.1029/2003GL017336, 2003.
- Anderson, T. L., D. S. Covert, J. D. Wheeler, J. M. Harris, K. D. Perry, B. E. Trost, and D. A. Jaffe, Aerosol backscatter fraction and single scattering albedo: Measured values and uncertainties at a coastal station in the Pacific Northwest, *J. Geophys. Res.*, *104*, 26,793-26,807, 1999.
- Atherton, C. S., S. Sillman, and J. Walton, Three-dimensional global modeling studies of the transport and photochemistry over the North Atlantic Ocean, *J. Geophys. Res.*, *101*, 29,289, 29,304, 1996.
- Barth, M. C., P. G. Hess, and S. Madronich, Effect of marine boundary layer clouds on tropospheric chemistry as analyzed in a regional chemistry transport model, *J. Geophys. Res.*, *107*(D11), 4126, doi:10.1029/2001JD000468, 2002.
- Bertschi, I. T., D. A. Jaffe, L. Jaeglé, H. U. Price, and J. B. Dennison, PHOBEA/ITCT 2002 Airborne observations of trans-Pacific transport of ozone, CO, VOCs and aerosols to the northeast Pacific: impacts of Asian anthropogenic and Siberian boreal fire emissions, *J. Geophys. Res.*, submitted, 2003.
- Bey, I., D. J. Jacob, J. A. Logan, and R. M. Yantosca, Asian chemical outflow to the Pacific in spring: origins, pathways, and budgets. *J. Geophys. Res.*, *106*, 23,097–23,113, 2001a.
- Bey, I., D. J. Jacob, R. M. Yantosca, J. A. Logan, B. D. Field, A. M. Fiore, Q. Li, H. Y. Liu, L. J. Mickley, and M. G. Schultz, Global modeling of tropospheric chemistry with assimilated

- meteorology: Model description and evaluation, *J. Geophys. Res.*, *106*, 23,073-23,096, 2001b.
- Carmichael, G. R., I. Uno, M. J. Phadnis, Y. Zhang, and Y. Sunwoo, Tropospheric ozone production and transport in the springtime in east Asia, *J. Geophys. Res.*, *103*, 10,649-10,671, 1998.
- Chin, M., D. J. Jacob, J. W. Munger, D. D. Parrish, and B. G. Doddridge, Relationship of ozone and carbon monoxide over North America, *J. Geophys. Res.*, *99*, 14,565-14,573, 1994.
- Derwent, R. G., P. G. Simmonds, S. Seuring, and C. Dimmer, Observation and interpretation of the seasonal cycles in the surface concentrations of ozone and carbon monoxide at Mace Head, Ireland from 1990 to 1994, *Atmos. Environ.*, *32*, 145– 157, 1998.
- Dickerson, R. R., K. P. Rhoads, T. P. Carsey, S. J. Oltmans, J. P. Burrows, and P. J. Crutzen, Ozone in the remote marine boundary layer: A possible role for halogens, *J. Geophys. Res.*, *104*, 21,385– 21,395, 1999.
- Duncan, B. N., R. V. Martin, A. C. Staudt, R. Yevich, and J. A. Logan, Interannual and seasonal variability of biomass burning emissions constrained by satellite observations, *J. Geophys. Res.*, *108*(D2), 4100, doi:10.1029/2002JD002378, 2003a.
- Duncan, B., J. A. Logan, I. Bey, R. V. Martin, D. J. Jacob, and R. M. Yantosca, Model study of the variability and trends of carbon monoxide (1988 - 1997): 1. Model formulation, evaluation, and sensitivity, submitted to *J. Geophys. Res.* (manuscript in preparation), 2003b.
- Elliot, S., D. R. Blake, R. A. Duce, C. A. Lai, I McCreary, L. A. McNair, F. S. Rowland, A. G. Russel, G. E. Streit, and R. P. Turco, Motorization of China implies changes in Pacific air chemistry and primary production, *Geophys. Res. Lett.*, *24*, 2671-2674, 1997.

- Fiore, A. M., D. J. Jacob, I. Bey, R. M. Yantosca, B. D. Field, A. C. Fusco, and J. G. Wilkinson, Background ozone over the United States in summer: Origin, trend, and contribution to pollution episodes, *J. Geophys. Res.*, *107*(D15), 10.1029/2001JD000982, 2002.
- Fuelberg, H. E., R. O. Jr Loring, M. V. Watson, M. C. Sinha, K. E. Pickering, A. M. Thompson, G. W. Sachse, D. R. Blake, and M. R. Schoeberl, TRACE A trajectory intercomparison, 2, Isentropic and kinematic methods, *J. Geophys. Res.*, *101*, 23,927-23,939, 1996.
- Fuelberg, H. E., C. M. Kiley, J. R. Hannan, D. J. Westberg, M. A. Avery, and R. E. Newell, Meteorological conditions and transport pathways during the Transport and Chemical Evolution over the Pacific (TRACE-P) experiment, *J. Geophys. Res.*, *108*(D20), 8782, doi:10.1029/2002JD003092, 2003.
- Harris, J. M. and J. D. W. Kahl, An analysis of 10-day Isentropic Flow Patterns for Barrow, Alaska: 1985-1992, *J. Geophys. Res.*, *99*, 25845 - 25855, 1994.
- Harris J. M., E. J. Dlugokencky, S. J. Oltmans, P. P. Tans, T. J. Conway, P. C. Novelli, and K. W. Thoning, An interpretation of trace gas correlations during Barrow, Alaska, winter dark periods, 1986-1997, *J. Geophys. Res.*, *105*, 17267-17278, 2000.
- He, S., and G. R. Carmichael, Sensitivity of photolysis rates and ozone production in the troposphere to aerosol properties, *J. Geophys. Res.*, *104*, 26,307– 26,324, 1999.
- Herring, J. A., D. A. Jaffe, H. J. Beine, S. Madronich, and D. R. Blake, High-latitude springtime photochemistry. Part II: Sensitivity studies of ozone production, *J. Atmos. Chem.*, *27*, 155-178, 1997.
- Holloway, T., H. Levy II, and P. Kasibhatla, Global distribution of carbon monoxide, *J. Geophys. Res.*, *105*, 12,123-12,147, 2000.

- Huebert, B., T. Bates, P. Russell, J. Seinfeld, M. Wang, M. Uematsu, and Y. J. Kim, An overview of ACE-Asia: Strategies for quantifying the relationships between Asian aerosols and their climatic impacts, *J. Geophys. Res.*, *108*, doi:10.1029/2003JD003550, in press, 2003.
- HYSPLIT, 1997. NOAA Air Research Laboratory, Silver Spring, MD, Web:  
<http://www.arl.noaa.gov/ready/hysplit4.html>.
- Jacob, D. J., J. A. Logan, and P. P. Murti, Effect of rising Asian emission on surface ozone in the United States. *Geophys. Res. Lett.*, *26*, 2175–2178, 1999.
- Jacob, D. J., J. H. Crawford, M. M. Kleb, V. E. Connors, R. J. Bendura, J. L. Raper, et al., The Transport and Chemical Evolution over the Pacific (TRACE-P) mission: Design, execution, and overview of results, *J. Geophys. Res.*, *108*(D20), 9000, doi:10.1029/2002JD003276, 2003.
- Jaegle, L., D. A. Jaffe, H. U. Price, P. Weiss-Penzias, P. I. Palmer, M. J. Evans, D. J. Jacob, and I. Bey, Sources and budgets for CO and O<sub>3</sub> in the northeastern Pacific during the spring of 2001: Results from the PHOBEA-II Experiment, *J. Geophys. Res.*, *108*(D20), 8802, doi:10.1029/2002JD003121, 2003.
- Jaffe, D. A., L. N. Yurganov, E. Pullman, J. Reuter, A. Mahura, and P. C. Novelli, Measurements of CO and O<sub>3</sub> at Shemya, Alaska, *J. Geophys. Res.*, *103*, 1493-1502, 1998.
- Jaffe, D. A., T. Anderson, D. Covert, R. Kotchenruther, B. Trost, J. Danielson, W. Simpson, T. Berntsen, S. Karlsdottir, D. Blake, J. Harris, G. Carmichael, and I. Uno, Transport of Asian air pollution to North America. *Geophys. Res. Lett.*, *26*, 711–714, 1999.
- Jaffe, D. A., T. Anderson, D. Covert, B. Trost, J. Danielson, W. Simpson, D. Blake, J. Harris, and D. Streets, Observations of ozone and related species in the northeast Pacific during

- the PHOBEA campaigns: 1. Ground based observations at Cheeka Peak. *J. Geophys. Res.*, *106*, 7449–7461, 2001.
- Jaffe, D. A., I. McKendry, T. Anderson, and H. Price, Six ‘new’ episodes of trans-Pacific transport of air pollutants, *Atmos. Environ.*, *37*, 391-404, 2003a
- Jaffe, D., H. Price, D. Parrish, A. Goldstein, and J. Harris, Increasing background ozone during spring on the west coast of North America, *Geophys. Res. Lett.*, *30*(12), 1613, doi:10.1029/2003GL017024, 2003b.
- Kotchenruther, R. A., D. A. Jaffe, H. J. Beine, T. L. Anderson, J. W. Bottenheim, J. M. Harris, D. R. Blake, and R. Schmitt, Observations of ozone and related species in the northeast Pacific during the PHOBEA campaigns. 2. Airborne observations, *J. Geophys. Res.*, *103*, 7463-7483, 2001a
- Kotchenruther, R., D. Jaffe, and L. Jaeglé, Ozone photochemistry and the role of peroxyacetyl nitrate in the springtime northeastern Pacific troposphere: Results from the Photochemical Ozone Budget of the Eastern North Pacific Atmosphere (PHOBEA) campaign, *J. Geophys. Res.*, *106*, 28,731–28,742, 2001b.
- Kunz, H., and P. Speth, Variability of near-ground ozone concentrations during cold front passages – a possible effect of tropopause folding events, *J. Atmos. Chem.*, *28*, 77-95, 1997.
- Langmann, B., S. E. Bauer, and I. Bey, The influence of the global photochemical composition of the troposphere on European summer smog, Part I, Application of a global to mesoscale model chain, *J. Geophys. Res.*, *108*(D4), 4146, doi:10.1029/ 2002JD002072, 2003.

- Lawrence, M. G., and P. J. Crutzen, Influence of NO<sub>x</sub> emissions from ships on tropospheric photochemistry and climate, *Nature*, 402, 167-170, 1999.
- Lelieveld, J., and F. J. Dentener, What controls tropospheric ozone? *J. Geophys. Res.*, 105, 3531-3551, 2000.
- Li, Q., D. J. Jacob, I. Bey, P. I. Palmer, B. N. Duncan, B. D. Field, R. V. Martin, A. M. Fiore, R. M. Yantosca, D. D. Parrish, P. G. Simmonds, and S. J. Oltmans, Transatlantic transport of pollution and its effects on surface ozone in Europe and North America, *J. Geophys. Res.*, 107 (D13), 10.1029/2001JD001422, 2002.
- Liang, Q., L. Jaeglé, D. A. Jaffe, P. Weiss-Penzias, A. Heckman, and J. A. Snow, Long-range transport of Asian pollution to the northeast Pacific: seasonal variations and transport pathways of carbon monoxide, accepted, *J. Geophys. Res.*, 2004.
- Liu, H., D. J. Jacob, I. Bey, R. M. Yantosca, B. N. Duncan, and G. W. Sachse, Transport pathways for Asian pollution outflow over the Pacific: Interannual and seasonal variations, *J. Geophys. Res.*, 108(D20), 8786, doi:10.1029/2002JD003102, 2003.
- Liu, S. C., M. Trainer, F. C. Fehsenfeld, D. D. Parrish, E. J. Williams, D. W. Fahey, G. Hubler, and P. C. Murphy, Ozone production in the rural troposphere and the implications for regional and global ozone distributions, *J. Geophys. Res.*, 92, 4191-4207, 1987.
- Mauzerall, D. L., D. Narita, H. Akimoto, L. Horowitz, S. Walters, D. Hauglustaine, and G. Brasseur, Seasonal characteristics of tropospheric ozone production and mixing ratios over East Asia: A global three-dimensional chemical transport model analysis, *J. Geophys. Res.*, 105, 17,895-17,910, 2000.
- Merrill, J. T., Isentropic airflow probability analysis, *J. Geophys. Res.*, 99, 25881-25889, 1994.

- Moody, J. L., S. J. Oltmans, H. Levy II, and J. T. Merrill, Transport climatology of tropospheric ozone: Bermuda, 1988–1991, *J. Geophys. Res.*, *100*, 7179–7194, 1995.
- Newell, R. E., and M. J. Evans, Seasonal changes in pollutant transport to the North Pacific: The relative importance of Asian and European sources, *Geophys. Res. Lett.*, *27*, 2509– 2512, 2000.
- Novelli, P. C., L. P. Steele, and P. P. Tans, Mixing ratios of carbon monoxide in the troposphere, *J. Geophys. Res.*, *97*, 20,731-20,750, 1992.
- Novelli, P. C., K. A. Masarie, and P. M. Lang, Distributions and recent changes of carbon monoxide in the lower troposphere, *J. Geophys. Res.*, *103*, 19,015-19,033, 1998.
- Oltmans, S. J., and H. Levy II, Surface ozone measurements from a global network, *Atmos. Environ.*, *28*, 9-24, 1994.
- Parrish, D. D., M. Trainer, J. S. Holloway, J. E. Yee, M. S. Warshawsky, F. C. Fehsenfeld, G. L. Forbes, and J. L. Moody, Relationships between ozone and carbon monoxide at surface sites in the North Atlantic region, *J. Geophys. Res.*, *103*, 13,357– 13,376, 1998.
- Parrish, D. D., et al., *J. Geophys. Res.*, submitted, 2004
- Pickering, K. E., A. M. Thompson, D. P. McNamara, M. R. Schoeberl, H. E. Fuelberg, R. O. Jr. Loring, M. V. Watson, K. Fakhruzzaman, and A. S. Bachmeier, TRACE A trajectory intercomparison, 1, Effects of different input analyses, *J. Geophys. Res.*, *101*, 23,909-23,925, 1996.
- Pochanart, P., H. Akimoto, Y. Kajii, V. M. Potemkin, and T. V. Khodzher, Regional background ozone and carbon monoxide variations in remote Siberia/East Asia, *J. Geophys. Res.*, *108*(D1), 4028, doi:10.1029/2001JD001412, 2003.

- Price, H. U., D. A. Jaffe, P. V. Doskey, I. McKendry, and T. Anderson, Vertical profiles of O<sub>3</sub>, aerosols, CO and NMHCs in the Northeast Pacific during the TRACE-P and ACE-ASIA experiments, *J. Geophys. Res.*, 108(D20), 8799, doi:10.1029/2002JD002930, 2003.
- Price, H. U., D. A. Jaffe, O. Cooper, and P. V. Doskey, Photochemistry, ozone production and dilution during long-range transport episodes from Eurasia to the Northwest U. S., *J. Geophys. Res.*, accepted, 2004.
- Simmonds, P. G., S. Seuring, G. Nickless, and R. G. Derwent, Segregation and interpretation of ozone and carbon monoxide measurements by air mass origin at the TOR station Mace Head, Ireland from 1987 to 1995, *J. Atmos. Chem.*, 28, 45-59, 1997.
- Song, C. H., G. Chen, S. R. Hanna, J. Crawford, and D. D. Davis, Dispersion and chemical evolution of ship plumes in the marine boundary layer: Investigation of O<sub>3</sub>/NO<sub>y</sub>/HO<sub>x</sub> chemistry, *J. Geophys. Res.*, 108(D4), 4143, doi:10.1029/2002JD002216, 2003.
- Staudt, A. C., D. J. Jacob, J. A. Logan, D. Bachiochi, T. N. Krishnamurti, and G. W. Sachse, Continental sources, transoceanic transport, and interhemispheric exchange of carbon monoxide over the Pacific, *J. Geophys. Res.*, 106, 32,571-32,590, 2001.
- Stohl, A., Computation, accuracy and applications of trajectories—a review and bibliography, *Atmos. Environ.*, 32 (6), 947–966, 1998.
- Streets, D. G., and S. T. Waldhoff, Present and future emissions of air pollutants in China: SO<sub>2</sub>, NO<sub>x</sub>, and CO, *Atmos. Environ.*, 34, 363-374, 2000.
- Weiss-Penzias, P., D. A. Jaffe, A. McClintick, E. M. Prestbo, and M. S. Landis, Gaseous elemental mercury in the marine boundary layer: evidence for rapid removal in anthropogenic pollution, *Environ. Sci. Technol.*, 37, 3755-3763, 2003.

Yienger, J. J., M. Galanter, T. A. Holloway, M. J. Phandis, S. K. Guttikinda, G. R. Carmichael, W. J. Moxim, and H. Levy II, The episodic nature of air pollution transport from Asia to North America, *J. Geophys. Res.* *105*, 26,931-26,945, 2000.

## Figure Captions

Figure 1: Location of CPO on the western coast of North America and the trajectory classifications based on air position criteria explained in text.

Figure 2: A) Measured CO ( $CO_{\text{meas}}$ ) and  $O_3$  ( $O_{3\text{ meas}}$ ), and modeled CO ( $CO_{\text{mod}}$ ) monthly means and standard deviations at CPO during PHOBEA I-II. Both model and measurements have been screened for “marine-only” periods. B) Model generated medians of CO from three sources. “LRT” = Asian biomass burning + Asian and European fossil- and bio-fuel combustion, “Oxidation-CO” = oxidation of hydrocarbons, and “NA” = fossil fuel combustion from North America.

Figure 3: Histograms of LRT CO values for each month, using 6-hour averaged marine-only LRT data. The median, 75<sup>th</sup> and 25<sup>th</sup> percentiles are shown, which correspond to the data in Table 2. Note the different y-axis scale for July.

Figure 4: Monthly averages of (A) measured CO and (B) measured  $O_3$  concentrations segregated by the amount of “LRT” predicted by GEOS-CHEM. The inset graphs show the difference in CO and  $O_3$  concentrations between the high (>75<sup>th</sup> percentile) and low (<25<sup>th</sup> percentile) LRT categories.

Figure 5: Monthly averages of (A) measured CO and (B) measured  $O_3$  concentrations segregated with isentropic back trajectories, defined by the regions shown in Figure 1. The inset graphs show the difference in CO and  $O_3$  concentrations between the “Asian” and “subtropical” categories. Data gaps in the inset graphs represent months where no “Asian” trajectories were classified.

Figure 6: CO and  $O_3$  measurements from 2-week period in April/May 2001, compared with GEOS-CHEM model results and isentropic and Hysplit trajectory classifications. No “marine-only” screening was done to these data. Trajectory classifications were given numbers: 1 = local, 2 = North Pacific (NP), 3 = Asian (As), 4 = subtropical (ST). See Figure 1 for region definitions. Events “a”, “b”, “c”, and “d” are specific comparison periods discussed in the text.

Figure 7: Slope ( $\Delta O_3/\Delta CO$  in ppbv/ppbv) vs. correlation coefficient ( $r^2$ ) from “marine-only” measured  $O_3$  and CO 6-hour averages by month.

Figure 8: Diurnal cycles of “marine-only” measured  $O_3$ . LRT segregated data are shown for March and April only.

Table 1: Monthly means of CO and O<sub>3</sub> measurements and GEOS-CHEM model results from “marine-only” periods during the PHOBEA I and II campaigns. 6-hr averages were used for both the measurements and the model. ND refers to no CO measurements.

Month	# of hours “marine-only”, normalized by month	Measured CO (ppbv)	Measured O <sub>3</sub> (ppbv)	Total Modeled CO (ppbv)	Measured CO vs. Total Modeled CO Corr. Coeff. (r)
Jan	420	138	43.9	127	0.74
Feb	282	149	44.2	134	0.70
Mar	380	159	44.8	147	0.60
Apr	395	154	45.8	142	0.79
May	516	132	44.6	120	0.59
Jun	534	103	36.6	102	0.50
Jul	630	81	28.4	94	0.16
Aug	420	78	29.3	80	0.54
Sep	288	87	34.2	97	0.42
Oct	450	ND	41.4	109	ND
Nov	408	112	42.4	117	0.60
Dec	372	129	43.5	124	0.24
<b>Annual Average, Normalized</b>	<b>425 (59%)</b>	<b>120</b>	<b>39.9</b>	<b>116</b>	<b>0.53</b>

Table 2: The long-range transport (LRT) component from GEOS-CHEM, and its correlation with measured CO. All data are calculated using 6-hour averages. ND refers to no CO measurements.

Month	Measured CO vs. LRT Correlation (r)	LRT median (ppbv)	LRT 75 <sup>th</sup> pctl. (ppbv)	LRT 25 <sup>th</sup> pctl. (ppbv)	Difference between 75 <sup>th</sup> and 25 <sup>th</sup> pctl. (ppbv)
Jan	0.71	59	61	55	6
Feb	0.69	62	66	55	11
Mar	0.55	72	81	69	12
Apr	0.74	76	80	67	13
May	0.66	60	66	49	17
Jun	0.70	44	47	34	13
Jul	0.60	28	30	25	5
Aug	0.60	21	25	18	7
Sep	0.47	26	30	25	5
Oct	ND	42	45	39	6
Nov	0.47	48	51	43	8
Dec	0.37	53	56	50	6
<b>Annual Average, Normalized</b>	<b>0.60</b>	<b>49</b>	<b>53</b>	<b>44</b>	<b>9</b>

Table 3: Events of long-range transported pollution identified during the PHOBEA I-II campaigns at CPO, arranged chronologically, and compared to the GEOS-CHEM model results. See text for definition of events.  $\Delta\text{CO}$  refers to the maximum difference between a 6-hour average and the monthly mean.  $\Delta\text{O}_3$  refers to difference between the 6-hour average and the monthly mean, at the same time as the measured CO maximum. The seasons have been shaded incrementally from spring (lightest) to winter (darkest).

Event Date (midpoint, GMT)	# of hours LRT > 75	$\Delta\text{CO}$ (ppbv)			$\Delta\text{O}_3$ (ppbv)	Correlation (r)	
		Measured	Total Modeled <sup>a</sup>	LRT Modeled <sup>b</sup>		Modeled vs. Measured CO	Measured $\text{O}_3$ vs. CO
9-Mar-97	78	24	20	19	-3.2	0.33	-0.30
29-Mar-97	60	19	21	20	1.2	0.77	0.42
11-Mar-01	30	28	21	26	4.5	0.97	0.59
7-Apr-01	54	16	13	9	-0.8	0.64	-0.48
29-Apr-01	30	4	8	11	9.3	0.75	0.49
2-May-01	60	19	25	20	1.2	0.31	-0.10
12-Jul-01	48	5	27	3	-2.4	0.59	-0.23
16-Jul-01	54	7	4	6	-1.7	0.61	-0.09
28-Sep-01	78	18	20	9	2.2	0.75	-0.19
21-Nov-01	30	10	7	6	1.6	0.21	-0.05
5-Dec-01	54	16	13	14	-2.9	0.30	0.55
9-Jan-02	24	3	12	6	6.2	0.92	0.88
20-Jan-02	66	28	23	20	2.6	0.81	-0.13
27-Mar-02	24	24	22	28	2.1	0.79	-0.04
4-May-02	48	16	14	16	1.7	0.18	0.05
15-May-02	42	8	15	12	-6.4	0.24	-0.46
<b>All Events, Weighted by # of Hours</b>	<b>774</b>	<b>16</b>	<b>17</b>	<b>14</b>	<b>0.4</b>	<b>0.91</b>	<b>0.78</b>

<sup>a</sup> Total modeled CO

<sup>b</sup> LRT component of total modeled CO

Table 4: Events predicted by GEOS-CHEM but do not agree well with the observations. Under “Reasons for Disagreement”, “M” refers to a lack of significant increase in measured CO, and “C” refers to poor correlation between model and measurement. The definition of  $\Delta\text{CO}$  and the shading by season is identical to that in Table 4. 6-hour averages were used to calculate r.

Event Date (midpoint, GMT)	# of hours LRT > 75%	$\Delta\text{CO}$ (ppbv)			Modeled vs. Measured CO Correlation	Reason for Disagreement
		Measured	Total Modeled	LRT Modeled		
20-Mar-97	30	-5	12	13	0.94	M
2-Apr-01	36	23	16	6	-0.13	C
11-Jun-01	72	9	18	21	0.02	C
4-Aug-01	30	2	16	7	-0.07	M, C
24-Aug-01	54	15	21	7	-0.77	C
23-Apr-02	48	19	21	20	-0.75	C

Table 5: Number of hours during long-range transport events that were classified as “Asian” by isentropic and Hysplit kinematic trajectories, in comparison to the number of hours LRT > 75%. The totals for each season are given in hours and in the percent of LRT > 75% hours.

Event Date (midpoint, GMT)	# of hours LRT > 75%	# of Hours Isentropic	# of Hours Hysplit Kinematic
9-Mar-97	78	72	72
29-Mar-97	60	36	60
11-Mar-01	30	24	24
27-Mar-02	24	24	24
7-Apr-01	54	12	12
29-Apr-01	30	24	24
2-May-01	60	24	12
4-May-02	48	24	24
15-May-02	42	0	12
<i>Mar-Apr Total</i>	<i>276</i>	<i>192 (70%)</i>	<i>216 (78%)</i>
<i>Spring Total</i>	<i>426</i>	<i>240 (56%)</i>	<i>264 (62%)</i>
12-Jul-01	48	0	0
16-Jul-01	54	12	24
<i>Summer Total</i>	<i>102</i>	<i>12 (12%)</i>	<i>24 (24%)</i>
28-Sep-01	78	0	24
21-Nov-01	30	0	12
5-Dec-01	54	48	48
9-Jan-02	24	0	24
20-Jan-02	66	36	12
<i>Fall/Winter Total</i>	<i>252</i>	<i>84 (33%)</i>	<i>120 (48%)</i>
<b>All Events</b>	<b>774</b>	<b>336</b>	<b>408</b>

Table 6: A comparison of two types of disagreements in classifications using isentropic trajectories and GEOS-CHEM.  $\Delta\text{CO}_{\text{meas}}$  represents the average change from the monthly marine mean during the number of hours of each case. “—” corresponds to no occurrences of a disagreement, and ND refers to no CO measurements.

Month	“Asian” Isentropic Trajectories by Month	“Agreements” (“Asian” Isentropic & “LRT > 75%”)		"Disagreements" (“Asian” Isentropic & “LRT < 25%”)	
	(hrs)	(hrs)	$\Delta\text{CO}_{\text{meas}}$ (ppb)	(hrs)	$\Delta\text{CO}_{\text{meas}}$ (ppb)
Jan	48	12	13		
Feb	156	36	5	12	-7
Mar	102	60	12	9	-9
Apr	60	36	15	6	-13
May	42	42	10	--	--
Jun	0	--	--	--	--
Jul	12	12	0	--	--
Aug	0	--	--	--	--
Sep	0	--	--	--	--
Oct	96	36	ND	--	--
Nov	96	24	-5	48	-11
Dec	156	48	5	36	-6

Figure 1: Location of CPO on the western coast of North America and the trajectory classifications based on air position criteria explained in text.

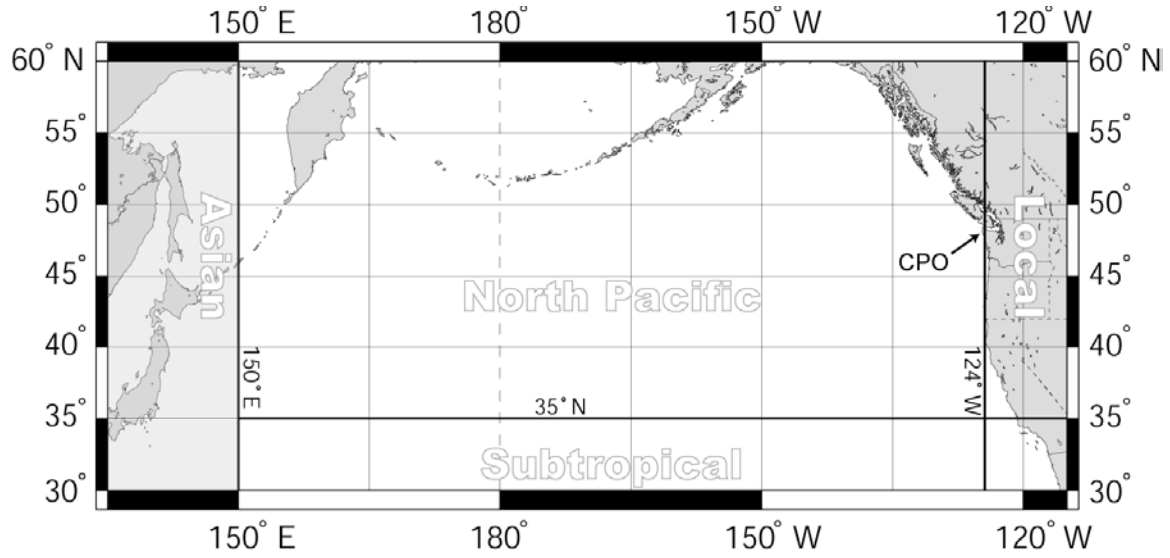


Figure 2: A) Measured CO ( $CO_{meas}$ ) and  $O_3$  ( $O_{3\ meas}$ ), and modeled CO ( $CO_{mod}$ ) monthly means and standard deviations at CPO during PHOBEA I-II. Both model and measurements have been screened for “marine-only” periods. B) Model generated medians of CO from three sources. “LRT” = Asian biomass burning + Asian and European fossil- and bio-fuel combustion, “Oxidation-CO” = oxidation of hydrocarbons, and “NA” = fossil fuel combustion from North America.

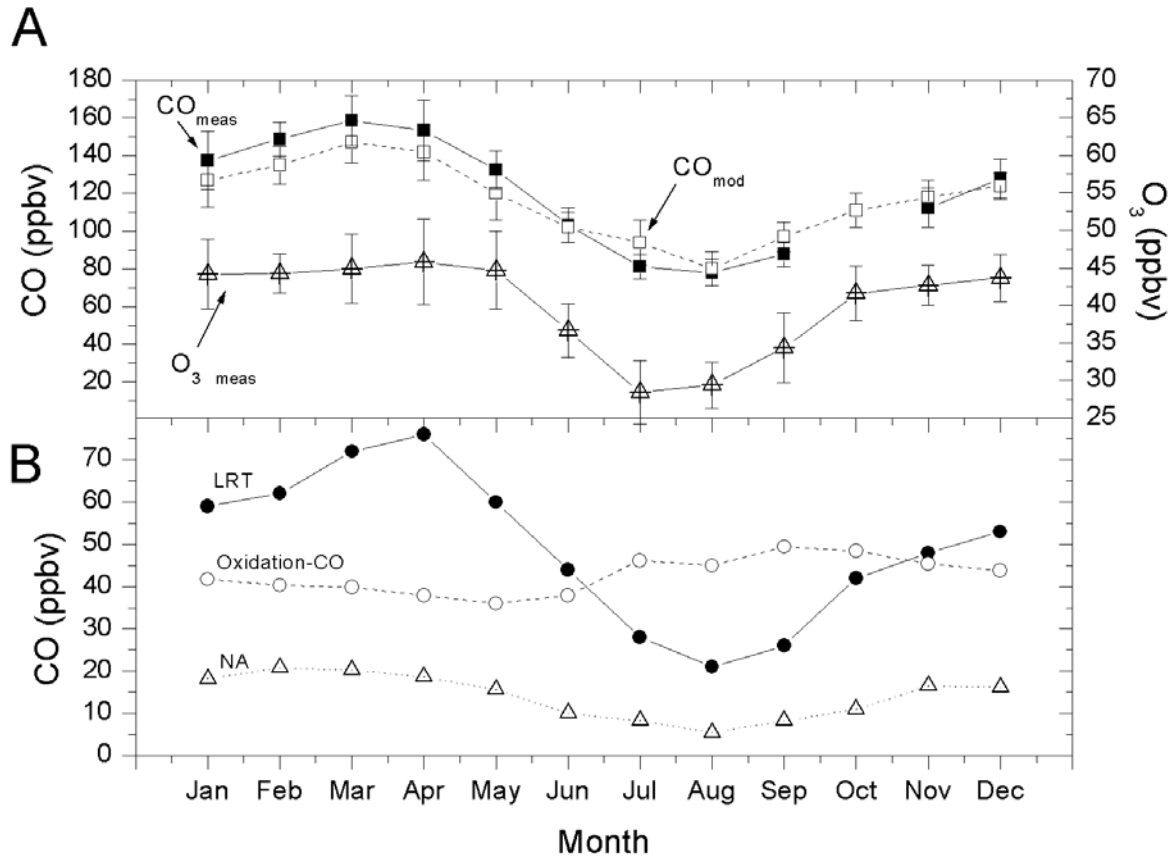


Figure 3: Histograms of LRT CO values for each month, using 6-hour averaged marine-only LRT data. The median, 75<sup>th</sup> and 25<sup>th</sup> percentiles are shown, which correspond to the data in Table 2. Note the different y-axis scale for July.

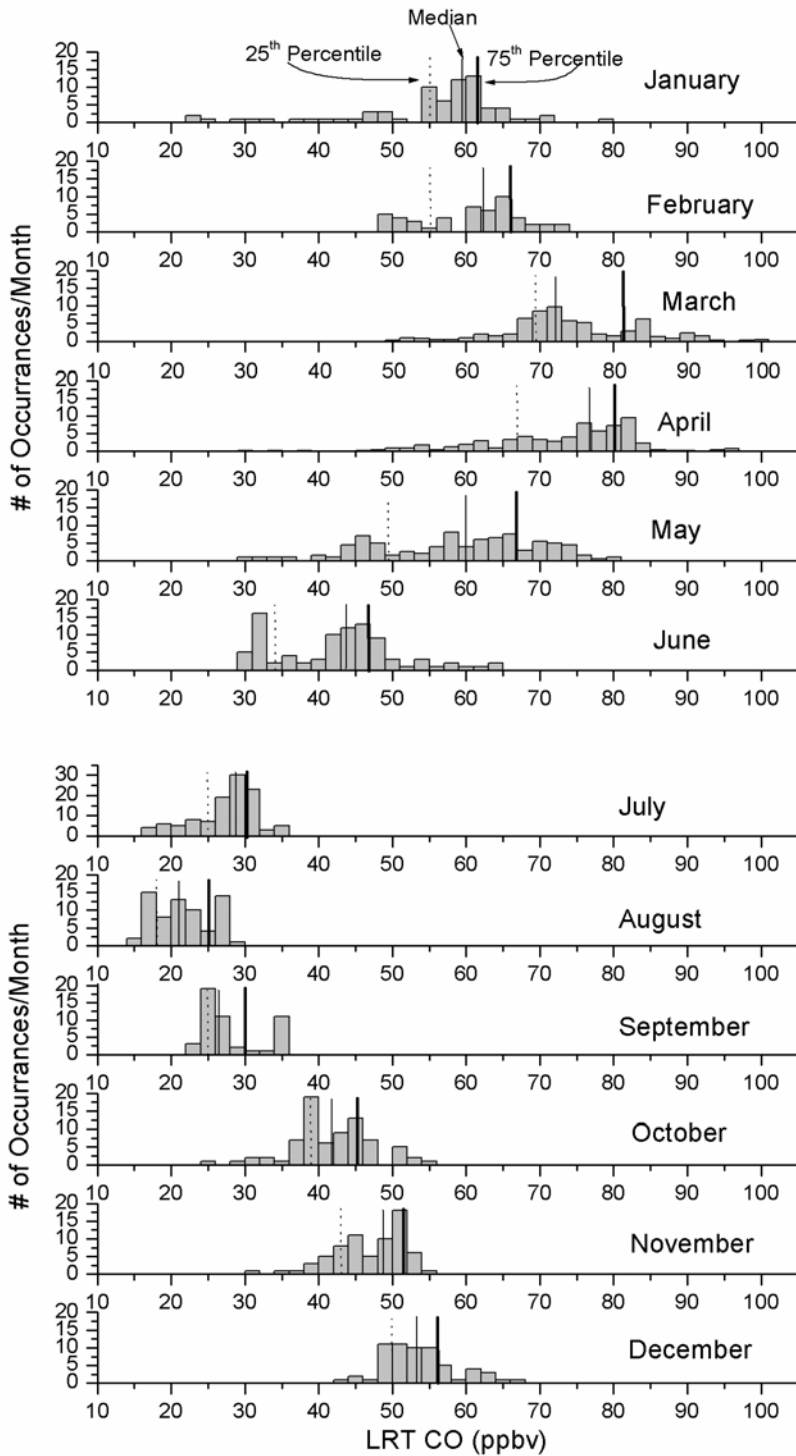


Figure 4: Monthly averages of (A) measured CO and (B) measured O<sub>3</sub> concentrations segregated by the amount of “LRT” predicted by GEOS-CHEM. The inset graphs show the difference in CO and O<sub>3</sub> concentrations between the high (>75<sup>th</sup> percentile) and low (<25<sup>th</sup> percentile) LRT categories.

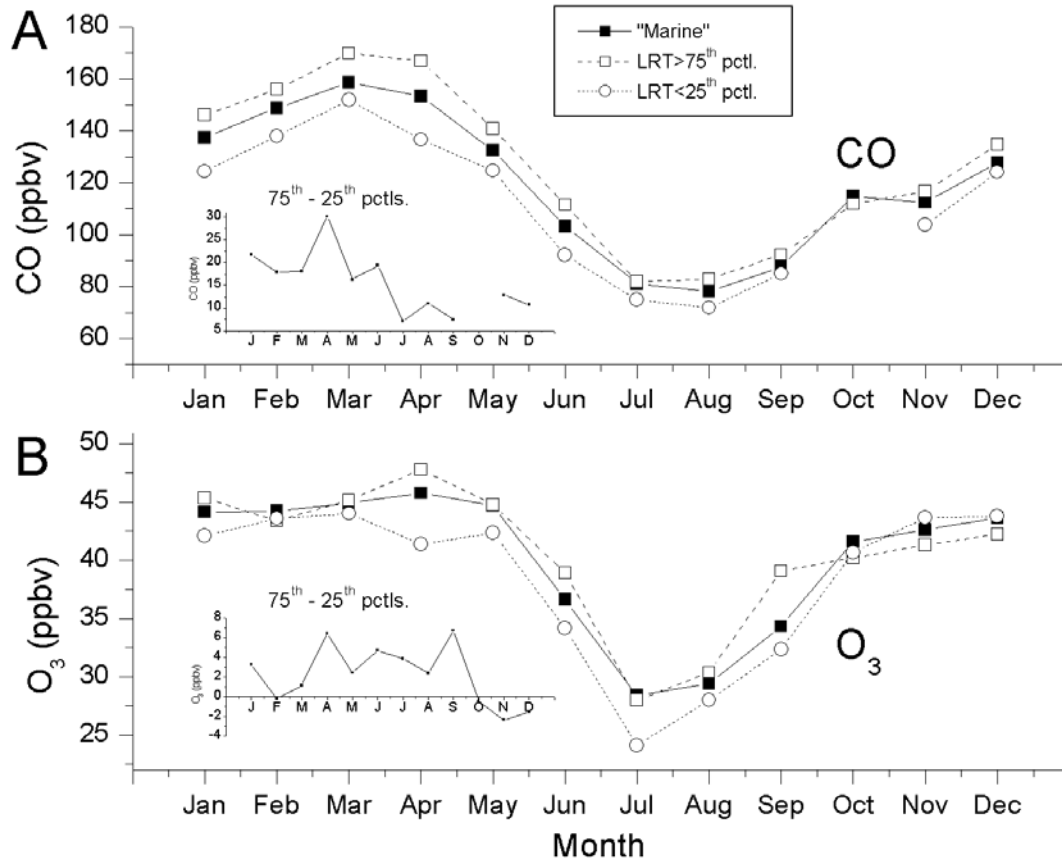


Figure 5: Monthly averages of (A) measured CO and (B) measured O<sub>3</sub> concentrations segregated with isentropic back trajectories, defined by the regions shown in Figure 1. The inset graphs show the difference in CO and O<sub>3</sub> concentrations between the “Asian” and “subtropical” categories. Data gaps in the inset graphs represent months where no “Asian” trajectories were classified.

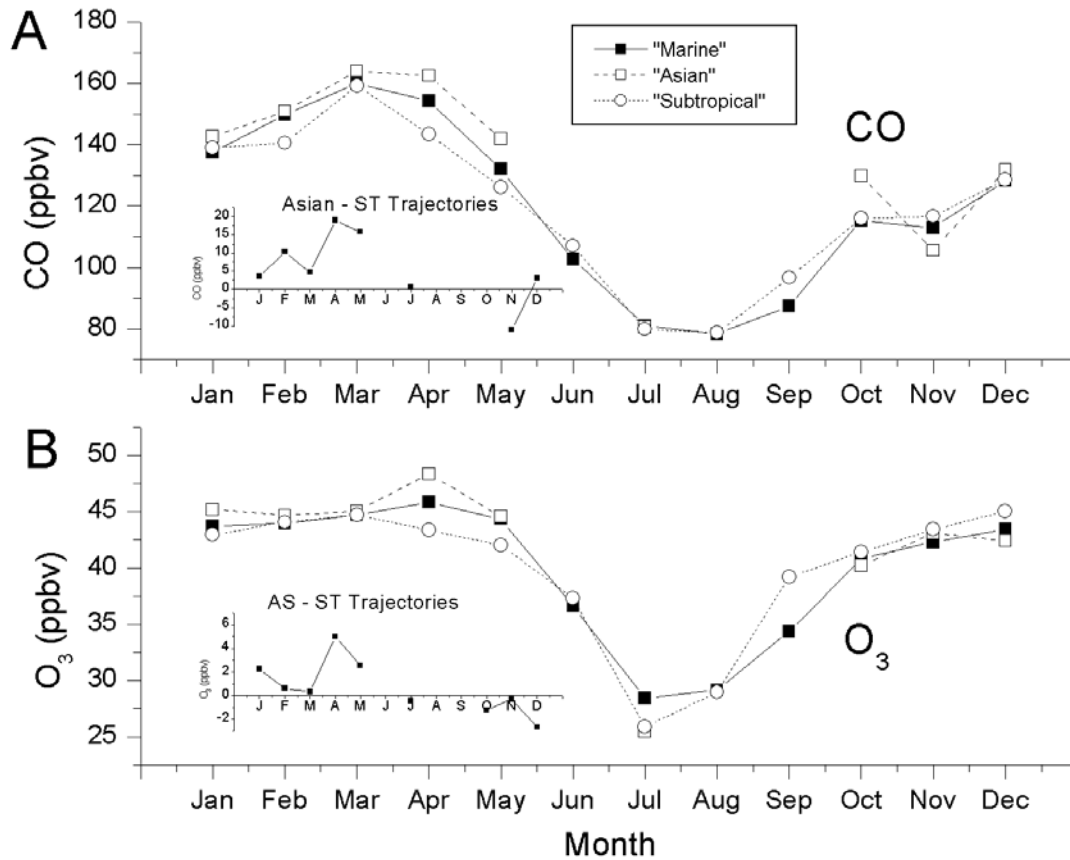


Figure 6: CO and O<sub>3</sub> measurements from 2-week period in April/May 2001, compared with GEOS-CHEM model results and isentropic and Hysplit trajectory classifications. No “marine-only” screening was done to these data. Trajectory classifications were given numbers: 1 = local, 2 = North Pacific (NP), 3 = Asian (As), 4 = subtropical (ST). See Figure 1 for region definitions. Events “a”, “b”, “c”, and “d” are specific comparison periods discussed in the text.

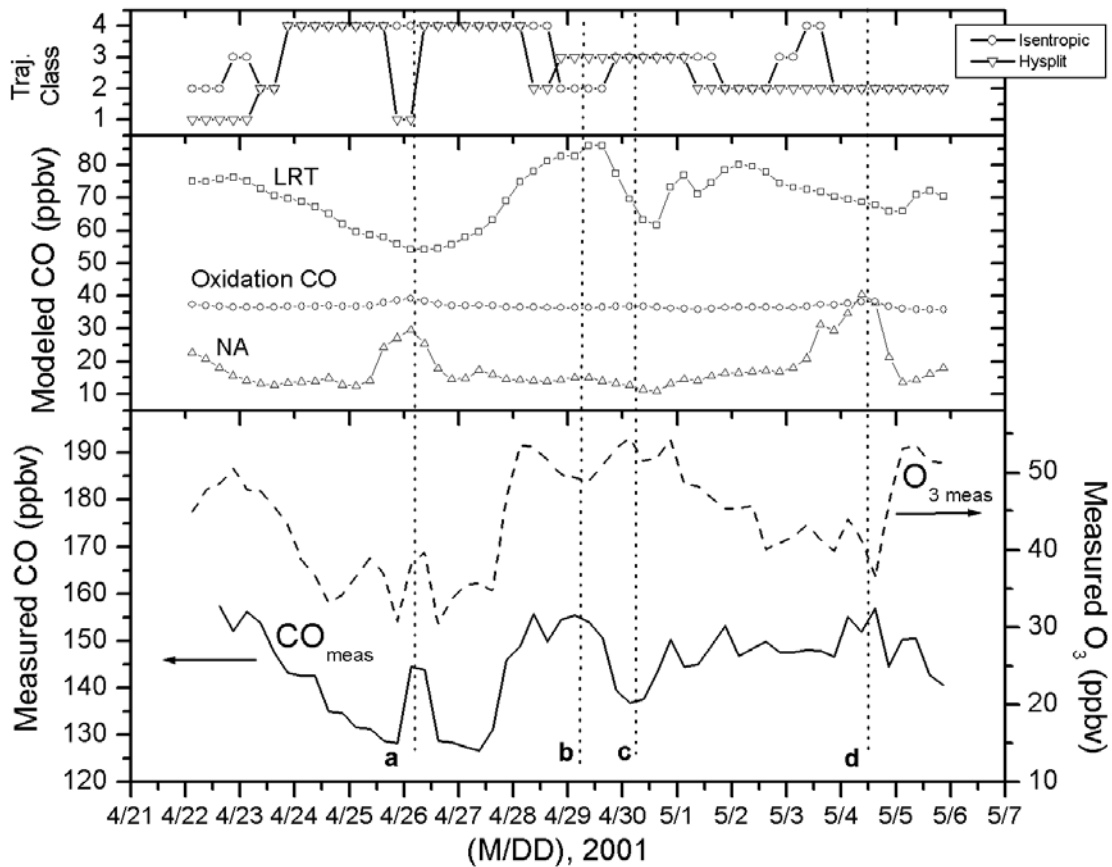


Figure 7: Slope ( $\Delta O_3/\Delta CO$  in ppbv/ppbv) vs. correlation coefficient ( $r^2$ ) from “marine-only” measured  $O_3$  and CO 6-hour averages by month.

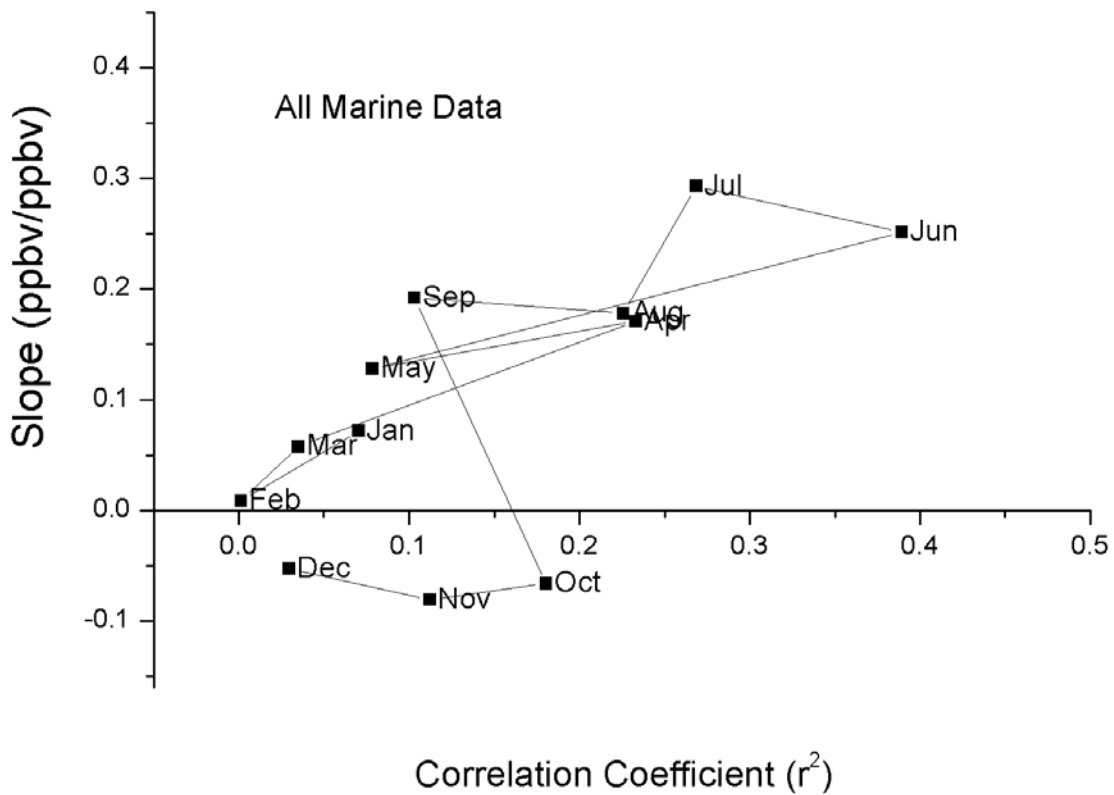


Figure 8: Diurnal cycles of “marine-only” measured O<sub>3</sub>. LRT segregated data are shown for March and April only.

